Validation of LQR control with integral action for a suspended four-cable-driven parallel robot

Yanis Tadjouddine[1], Atal Anil Kumar[1], Jean-François Antoine[1], Thibaut Raharijaona[1]

Abstract— **Many control strategies have been proposed for Cable-Driven Parallel Robots, but few have been experimentally validated, particularly for suspended four-cable architectures. This paper presents the design and experimental demonstration of a Linear Quadratic Regulator with integral action for a suspended four-cable parallel robot actuating a point mass. The proposed approach demonstrates that such systems can be controlled using a linear controller, without relying on nonlinear or predictive methods. A linearized dynamic model is derived around an equilibrium configuration, and the controller is implemented in discrete time using high-precision motion-capture feedback. We experimentally validated the control law on a prototype through planar and spatial trajectory tracking. Results demonstrate stable and accurate tracking, with root mean square (RMS) Cartesian errors below 0.044 m.**

Index Terms— **Cable-driven parallel robots, Linear Quadratic Regulator, Motion-Capture, Integral action.**

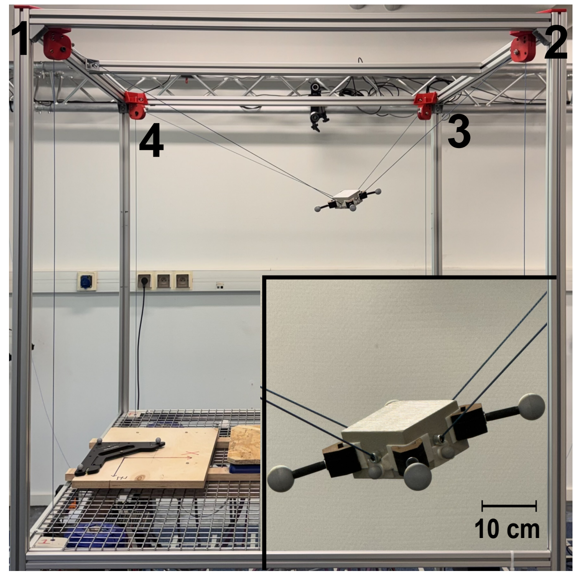

Fig. 1. Prototype of a suspended four-cable-driven robot with a point mass of $1.04\,\mathrm{kg}$, enclosed within a cubic frame of dimensions $1\,\mathrm{m}^3$.

I. Introduction

Cable-Driven Parallel Robots (CDPRs) offer lightweight architectures capable of high accelerations, making them suitable for applications requiring large workspaces and high flexibility, such as human-robot interaction and precision agriculture [1], [2], [3], [4]. Their control is constrained by unilateral cable tensions, configuration-dependent nonlinearities, and effects such as cable elasticity, friction, and actuator-platform coupling. In suspended configurations, particularly in four-cable systems, the dynamics are strongly influenced by gravity, which helps maintain cable tension but reduces the reachable workspace and increases sensitivity to disturbances and modeling errors [5], [6].

Control problem. We consider a suspended four-cable robot whose moving platform is modeled as a point mass (see Fig. 1). Its Cartesian position is $p = [x \;\; y \;\; z]^T$, and it is actuated by four cables that can only transmit positive and bounded tensions. We aim at designing a real-time feedback controller that computes cable tensions from measured Cartesian positions and converts them into cable length commands for the motors, in order to track a desired 3D trajectory while ensuring local stability and zero steady-state error.

Gap and motivation. A wide range of control strategies has been proposed for CDPRs, including classical PID-based schemes, nonlinear, robust, and model predictive approaches [7], [8], [9], [10]. These methods achieve stable tracking performance; but they often rely on accurate system modeling, computational resources, or extensive parameter tuning, which can limit their applicability in real-time experimental implementations, especially for suspended architectures with strong gravity-induced coupling. Recent work has also shown that modeling cable flexibility becomes necessary to achieve high bandwidth, making the system model more difficult to identify accurately [11].

Linear Quadratic Regulator (LQR) has been investigated in previous studies and has shown promising results, mainly in simulation, demonstrating the potential of linear optimal control for CDPR stabilization [12], [13], [14]. Its relevance in suspended CDPRs lies in its low computational cost and suitability for real-time implementation around an equilibrium point, while providing smooth control inputs that limit excessive actuator effort. However, most of these works remain theoretical or simulation-based, and experimental demonstrations on suspended four-cable systems are limited. This motivates the present work, which investigates the feasibility of linear optimal control for suspended CDPRs in real-time experimental conditions.

This paper presents the design, implementation, and experimental validation of an LQR controller with integral action for a suspended four-cable robot actuating a point mass. The LQR ensures local stability, while the integral action eliminates steady-state error in Cartesian position. A linearized dynamic model is derived around a chosen equilibrium point, and the controller is implemented in discrete time using high-precision motion-capture feedback. The method is validated

*This work was not supported by any organization.

[1] Authors are with Université de Lorraine, Arts et Metiers Institute of Technology, LCFC, F-57070 Metz, France
tadjou-junior-yanis.tadjouddine@univ-lorraine.fr

through planar and spatial trajectory tracking experiments.

Contributions. The main contributions of this work are:

- The development of an LQR controller with integral action for suspended four-cable CDPRs, based on a linearized point-mass model and implemented in discrete time using high-precision motion-capture feedback.
- The experimental demonstration that linear optimal control is sufficient to achieve stable and accurate 3D trajectory tracking of a suspended four-cable CDPR, despite strong gravity-induced coupling and unilateral cable tension constraints.

II. Experimental setup

We conducted the experimental validation on a CDPR prototype developed at the LCFC (Laboratoire de Conception Fabrication Commande) laboratory. The robot uses four base-mounted motor–winch units (Maxon EC-i 52 brushless) to control the cable lengths. The platform is modeled as a point mass of $1.04\,\mathrm{kg}$, as shown in Fig. 2B. Its position is measured using an OptiTrack motion capture system with ten Flex 13 cameras and reflective markers, providing sub-millimeter positional accuracy depending on the camera configuration and marker placement.

Position data are recorded at $120\,\mathrm{Hz}$ in MATLAB through Motive software and the NatNet SDK for real-time streaming. Communication between the PC and the Maxon EPOS4 controllers is established via a USB-to-CAN interface (Innomaker USB2CAN) operating at $1\,\mathrm{Mbit/s}$ for real-time control and trajectory transmission. Control and data acquisition are implemented in Matlab/Simulink. The prototype includes eight pulleys guiding nylon cables ($1.6\,\mathrm{mm}$ diameter) and is enclosed in a cubic frame of dimensions $1\,\mathrm{m} \times 1\,\mathrm{m} \times 1\,\mathrm{m}$.

III. Methodology

A. Modeling

The platform is modeled as a point mass, as shown in Fig. 2. The cables are assumed rigid, massless, and straight, transmitting only tensile forces. With nylon cables and a $1\,\mathrm{kg}$ payload, cable deformation and sagging are negligible. The center of gravity is assumed to coincide with the geometric center of the reference frame. The platform attachment points are denoted by B_i, and the pulley exit points by A_i.

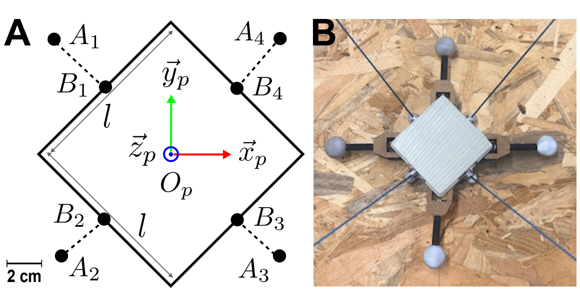

Fig. 2. Geometric model of the point mass: a $71.5 \times 71.5 \times 36\,\mathrm{mm}$ rectangular block of mass $1.04\,\mathrm{kg}$, with cables attached at the midpoints of its sides, forming a diamond configuration. **(A)** Top view showing geometric parameters. **(B)** Top view of the mass on the prototype, where eight reflective markers are used for position measurement with the OptiTrack system.

1) Geometric model: Let $\mathcal{R}_p = \{O_p, \overrightarrow{x_p}, \overrightarrow{y_p}, \overrightarrow{z_p}\}$ denote the reference frame attached to the point mass center (Fig. 2A), and l its dimension along the $\overrightarrow{x_p}$ and $\overrightarrow{y_p}$ axes. Let $\mathcal{R}_b = \{O_b, \overrightarrow{x_b}, \overrightarrow{y_b}, \overrightarrow{z_b}\}$ denote the base frame, and $p = [x \;\; y \;\; z]^T$ the Cartesian position. The positions of the attachment points B_i in $\mathcal{R}_b$ are:

$$^{b}b_i = p + \frac{l\sqrt{2}}{4}\,[1 \quad 1 \quad 0]^T, \quad i = 1,\dots,4, \tag{1}$$

The pulley geometry is used to determine the cable exit points A_i. Following [6], the point A_i is computed as:

$$^{b}a_i = {}^{b}d_i + e_i\left(\overrightarrow{u_i} + \overrightarrow{n_i}\right), \quad i = 1,\dots,4, \tag{2}$$

where $^{b}d_i$ is the cable entry point on the pulley, e_i the pulley radius, $\overrightarrow{u_i}$ the tangent vector along the groove, and $\overrightarrow{n_i}$ the normal to the pulley plane. Since $\overrightarrow{u_i}$ and $\overrightarrow{n_i}$ depend only on known geometric parameters, A_i can be computed directly.

Let $\overrightarrow{\rho_i}$ be the cable vector from the attachment point B_i to the pulley exit point A_i. One can write:

$$\overrightarrow{\rho_i} = {}^{b}a_i - {}^{b}b_i, \quad i = 1,\dots,4, \tag{3}$$

The cable lengths are then given by:

$$l_i(p) = \sqrt{\overrightarrow{\rho_i}^T \overrightarrow{\rho_i}} + e_i\left(\pi - \phi_i\right), \quad i = 1,\dots,4, \tag{4}$$

where ϕ_i is the cable exit angle on the pulley. The actuator position can then be determined from the cable length as:

$$q_i = C_0\left[l_i\left(p\right) - L_{i,0}\right], \quad i = 1,\dots,4, \tag{5}$$

where $C_0 = \dfrac{N.PPR}{2\pi r_b}$. PPR (Pulses Per Revolution) is the encoder resolution, r_b the winch radius, N the gearbox reduction ratio, and $L_{i,0}$ the initial cable length.

2) Dynamic model: The CDPR dynamics combine actuator and point-mass dynamics [15]. A simplified winch model is used [16], and all actuators are assumed identical. The actuator dynamics are then expressed as:

$$J_r\ddot{q} + f_v\dot{q} = \tau_m - f_s - \frac{r_b}{N}F \tag{6}$$

where q is the actuator position vector, J_r the inertia matrix of the rotor and the winch, τ_m the commanded motor torque vector, and f_v and f_s the viscous and static friction torque matrices, respectively. F is the cable tension vector acting on the mass, computed from Eq. (7).

The platform dynamics follow Newton–Euler equations. Since the platform is modeled as a point mass, the dynamic simplifies to [14]:

$$m_p\ddot{p} = \sum_{i=1}^{4} F_i t_i(p) - m_p g e_z - D\dot{p} \tag{7}$$

where m_p is the mass, g the gravity, e_z the unit vector along the z-axis, D the damping force, and F_i and t_i the cable tension and the corresponding unit direction vector, respectively.

The cable tension F_i is expressed as a function of the cable length l_i as follows:

$$F_i = k_i\left[l_i(p) - l_{i,0}\right], \quad i = 1,\dots,4, \tag{8}$$

where $l_{i,0}$ is the free length of the cable, i.e., its length when the tension is zero, and k_i the cable stiffness.

B. LQR controller with integral action design

The LQR is a state-feedback controller that minimizes a quadratic cost function involving both the system states and the control effort. It is well suited to coupled multi-variable systems such as CDPRs. The nonlinear point-mass dynamics are linearized around a chosen equilibrium point, and the controller is implemented in discrete time for real-time operation. The control architecture follows a cascaded structure (see Fig. 4), consisting of a fast inner loop operating at 1 kHz for actuator position control and a slower outer loop running at 10 Hz for Cartesian position control. An integral action is included to eliminate steady-state errors and improve tracking accuracy.

1) Mass dynamics linearization: Consider the system states $X = [x\ \dot{x}\ y\ \dot{y}\ z\ \dot{z}]^T$. The linearized model is expressed in state-space form using matrices A and B, obtained by differentiating the point-mass dynamics (Eq. (7)) with respect to the state variables around the equilibrium point. The matrices A and B are then given by:

$$A = \begin{bmatrix} 0 & 1 & 0 & 0 & 0 & 0 \\ \frac{\partial f_x}{\partial x} & -\frac{D}{m_p} & \frac{\partial f_x}{\partial y} & 0 & \frac{\partial f_x}{\partial z} & 0 \\ 0 & 0 & 0 & 1 & 0 & 0 \\ \frac{\partial f_y}{\partial x} & 0 & \frac{\partial f_y}{\partial y} & -\frac{D}{m_p} & \frac{\partial f_y}{\partial z} & 0 \\ 0 & 0 & 0 & 0 & 0 & 1 \\ \frac{\partial f_z}{\partial x} & 0 & \frac{\partial f_z}{\partial y} & 0 & \frac{\partial f_z}{\partial z} & -\frac{D}{m_p} \end{bmatrix} \quad (9)$$

$$B = \frac{1}{m_p} \begin{bmatrix} 0 & 0 & 0 & 0 \\ t_{1x} & t_{2x} & t_{3x} & t_{4x} \\ 0 & 0 & 0 & 0 \\ t_{1y} & t_{2y} & t_{3y} & t_{4y} \\ 0 & 0 & 0 & 0 \\ t_{1z} & t_{2z} & t_{3z} & t_{4z} \end{bmatrix} \quad (10)$$

where f denotes the point-mass dynamics in Eq. (7). Its derivative with respect to p is:

$$\frac{\partial f}{\partial p} = \frac{1}{m_p} \sum_{i=1}^{4} \overline{F_i} \frac{I_{3\times3} - t_i(\overline{p})\, t_i(\overline{p})^T}{\overline{l_i}} \quad (11)$$

where $I_{3\times3}$ is the 3×3 identity matrix, and $\overline{p}$, $\overline{F_i}$, and $\overline{l_i}$ represent the position, cable tension, and cable length at the equilibrium point, respectively.

2) Inner loop: The inner loop regulates the actuator angular position and is implemented in discrete time at 1 kHz ($T_e = 1\ ms$) using a proportional-derivative controller. The gains are tuned to obtain a damping ratio of 1 for the closed-loop second-order response, with a 10 ms time response. The block diagram is shown in Fig. 3. It includes both the actuator and point mass dynamics. Variables indexed by k denote the discrete-time counterparts of the continuous-time variables.

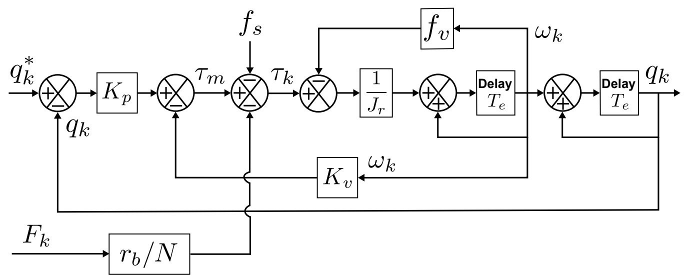

Fig. 3. Inner loop: actuator position control loop implemented in discrete time at 1 kHz using a proportional-derivative controller. It accounts for motor and point-mass dynamics via the cable tension input vector F.

3) Robot control scheme: The control design is based on the following discrete-time linearized model:

$$\begin{cases} \delta X_{k+1} = A_d \delta X_k + B_d \delta u_k, \\ y_k = C\, \delta X_k \end{cases} \quad (12)$$

with

$$C = \begin{bmatrix} 1 & 0 & 0 & 0 & 0 & 0 \\ 0 & 0 & 1 & 0 & 0 & 0 \\ 0 & 0 & 0 & 0 & 1 & 0 \end{bmatrix}$$

where $k \in \mathbb{N}$ denotes the discrete-time index, δX_k is the state deviation from the equilibrium point, δu_k is the control input computed by the outer-loop controller, and y_k is the Cartesian position of the mass. The matrices A_d and B_d are obtained by zero-order hold (ZOH) discretization of the continuous-time system with a sampling period T_s of 100 ms. C is the output matrix of the system.

To eliminate steady-state tracking errors, integral states η_k are included on the Cartesian position error as:

$$\eta_{k+1} = \eta_k + T_s\,(r_k - y_k)\,, \quad (13)$$

where r_k denotes the Cartesian reference position. The augmented state vector is defined as:

$$\overline{X}_k = \begin{bmatrix} \delta X_k \\ \eta_k \end{bmatrix} \quad (14)$$

The resulting augmented discrete-time system is [17]:

$$\overline{X}_{k+1} = \begin{bmatrix} A_d & 0 \\ -CA_d & I \end{bmatrix} \overline{X}_k + \begin{bmatrix} B_d \\ -CB_d \end{bmatrix} \delta u_k + \begin{bmatrix} 0 \\ T_s I \end{bmatrix} r_k \quad (15)$$

The LQR gain is obtained by minimizing the following quadratic cost function :

$$\hat{J}_c = \sum_{k=0}^{\infty} \left(\overline{X}_k^T Q \overline{X}_k + \delta u_k^T R \delta u_k \right) \quad (16)$$

where Q and R are positive semi-definite and positive definite weighting matrices, respectively. The solution of the discrete algebraic Riccati equation yields the optimal gain matrix K, leading to the following control law:

$$\delta u_k = -K\overline{X}_k, \quad \text{with} \quad K = [K_1\ K_2] \quad (17)$$

where K_1 corresponds to the state-feedback gains and K_2 to the integral gains. The overall control architecture is illustrated in Fig. 4. This cascaded architecture combines high-bandwidth actuator-level control with accurate Cartesian trajectory tracking.

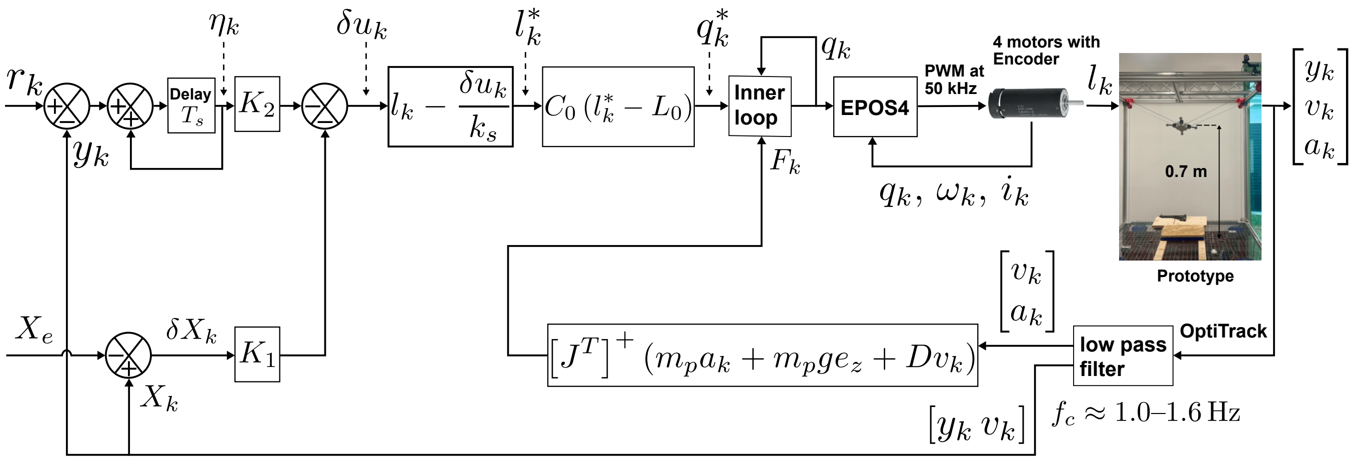

Fig. 4. Robot cascade control: Cartesian position control using an LQR with integral action, designed from the mass dynamics linearized around a chosen equilibrium point. The LQR outputs a tension command, which is converted into desired cable lengths via the cable stiffness model, and then into desired angular positions regulated by the inner loop. The LQR runs at $10\,\mathrm{Hz}$ using OptiTrack measurements at $120\,\mathrm{FPS}$, filtered with first-order low-pass filters (time constant below $150\,\mathrm{ms}$) to reduce vibrations. k_s denotes the cable stiffness matrix, X_e the equilibrium state, J^T the transpose of the Jacobian matrix, and v_k and a_k the Cartesian velocity and acceleration of the point mass, respectively.

4) Stability considerations: The linearized discrete-time model around the equilibrium point ($[0.5,\ 0.0,\ 0.020]^T$ m) is fully controllable, as confirmed by the controllability matrix, which has rank 9. The LQR controller derived from this model yields closed-loop eigenvalues located inside the unit circle, ensuring local asymptotic stability in discrete time.

IV. Results

The controller is designed around an equilibrium point corresponding to the initial position of the point mass, given by $[0.5,\ 0.0,\ 0.020]^T$ m. This equilibrium must remain sufficiently far from workspace boundaries, especially along the x and y axes, to avoid cable singularities and tension limits. The controller is first validated near this equilibrium and then tested on trajectories extending further away. It remains accurate within the operating range $x \in [0.2, 0.8]\,\mathrm{m}$, $y \in [-0.3, 0.3]\,\mathrm{m}$, and $z \in [0.010, 0.8]\,\mathrm{m}$; beyond these limits, the linear approximation loses validity and may lead to instability. Two representative trajectories are considered: a planar square trajectory and a spatial conical helical trajectory, shown in Figs. 5 and 6, respectively.

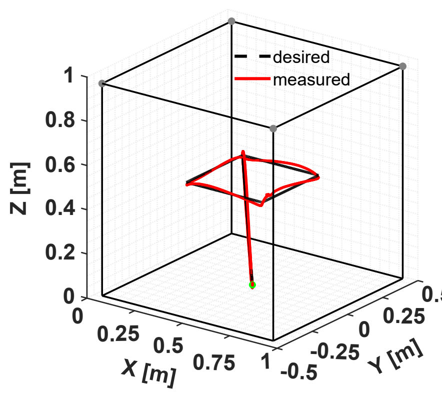

Fig. 5. 3D tracking of the mass along a square trajectory, showing desired and measured positions, with a root mean square error below $0.044\,\mathrm{m}$.

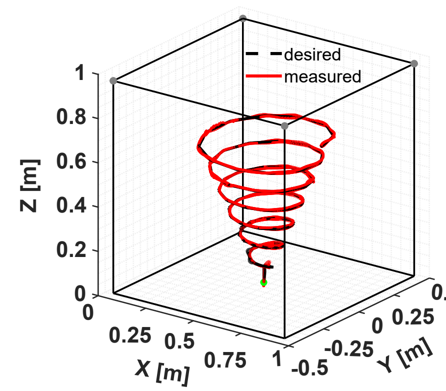

Fig. 6. 3D tracking of the mass along a helical trajectory, showing desired and measured positions, with a root mean square errors below $0.040\,\mathrm{m}$.

A. Controller parameters

The weighting matrices are chosen as $R = 16\,I_4$ and $Q = \mathrm{diag}(10^2,\ 1,\ 10^2,\ 1,\ 10^2,\ 1,\ 10^6,\ 10^6,\ 10^6)$. The maximum reference velocities are $6.1\,\mathrm{cm/s}$ for the square trajectory and $7.6\,\mathrm{cm/s}$ for the helical trajectory. The inner-loop gains, computed from the desired damping coefficient and response time, are $K_p = 90363$ and $K_v = 821.48$.

B. Cartesian tracking performance

For the square trajectory (Fig. 7), the point mass followed the reference path with zero steady-state Cartesian error and root mean square (RMS) tracking errors below 0.044 m. The RMS error is computed as the square root of the time-averaged squared Euclidean norm of the position error over the trajectory. Small transient deviations occurred during sharp direction changes, and a slight overshoot appeared along the z axis during the final descent due to gravity-assisted motion.

For the helical trajectory (Fig. 8), the robot maintained accurate tracking throughout the 8.6 min experiment. The ascent over six turns remained smooth and repeatable, while the descent reproduced the reference shape with minor

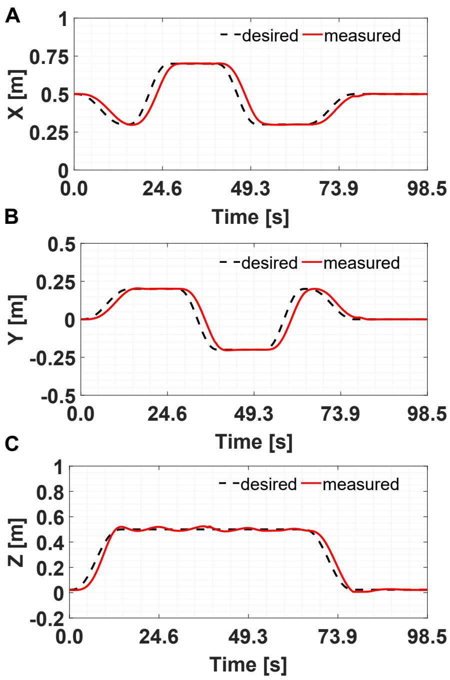

Fig. 7. Time evolution of the mass position during tracking of the square trajectory shown in Fig. 5. A small overshoot appeared in **C** due to gravity.

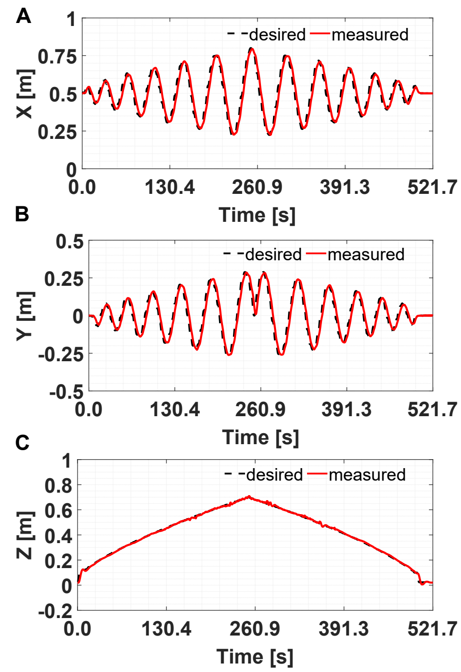

Fig. 8. Time evolution of the mass position during tracking of the square trajectory shown in Fig. 6. A small overshoot appeared in **C** due to gravity.

deviations. RMS tracking errors remained close to zero in steady state and below 0.040 m during transients.

The controller remains valid within the operating range defined in Sec. IV. Within this region, the linearized model accurately represents the system dynamics and ensures stable tracking. Outside these limits, nonlinear effects such as changes in cable directions and tension distribution increase tracking errors and may induce oscillations or instability.

C. Cable length and tension behavior

Figures 9 and 10 compare simulated and experimental cable lengths for the square and helical trajectories. RMS tracking errors remained below 0.02 m for the square trajectory and 0.017 m for the helical trajectory. The experimental curves followed the simulated trends, indicating that the stiffness-based cable model represents the dominant geometric and elastic effects relevant for control.

Cable tensions also remained consistent with simulation predictions for both trajectories (Figs. 11 and 12), with RMS tracking errors below 0.088 N for the square trajectory and 0.09 N for the helical trajectory. The tension profiles reproduced the expected variations due to changes in point mass position and cable geometry.

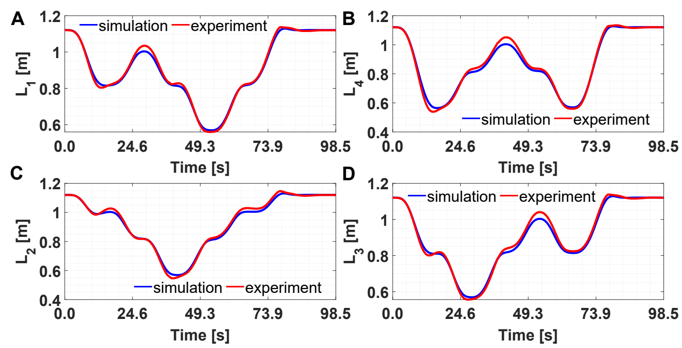

Fig. 9. Comparison of simulated and experimental cable lengths during tracking of the square trajectory, with RMS errors below $0.02\,$m.

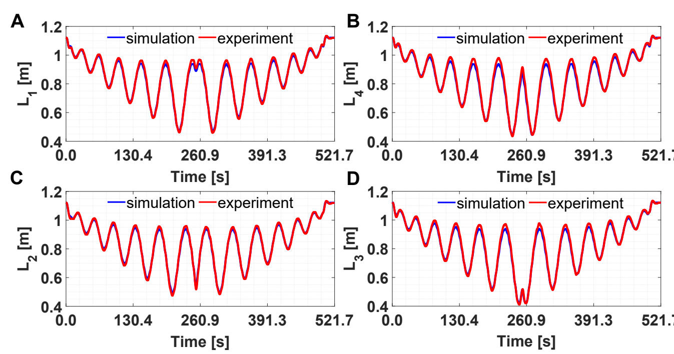

Fig. 10. Comparison of simulated and experimental cable lengths during tracking of the helical trajectory, with RMS errors below $0.017\,$m.

V. Discussion

The results show that an LQR controller with integral action, based on a linearized point-mass model, can regulate the motion of a four-cable CDPR, even in the presence of nonlinear effects such as workspace-dependent cable directions, unilateral tension constraints, and gravity. The controller achieved accurate tracking for both square and helical trajectories. The integral action eliminated steady-state errors, while stability remained even for motions away from the equilibrium point. Small overshoots during vertical motion are mainly due to gravity and dynamic transitions not captured by the linear model.

Transient delays during rapid motions are mainly due to the limited closed-loop bandwidth of the LQR controller, which results in increased phase lag for fast-varying trajectories. The bandwidth is first characterized using the Bode diagram of the transfer function, which provides information

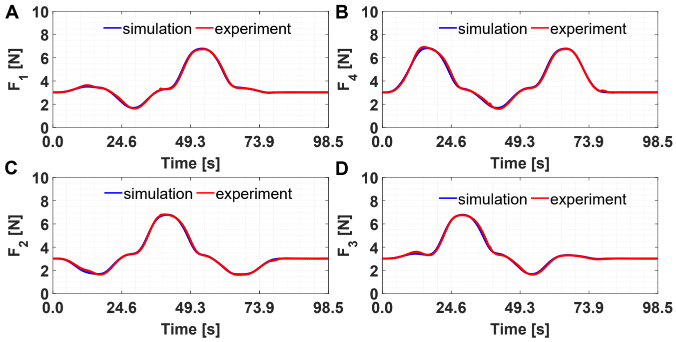

Fig. 11. Comparison of simulated and experimental cable tensions during tracking of the square trajectory, with RMS errors below $0.088\,\mathrm{N}$.

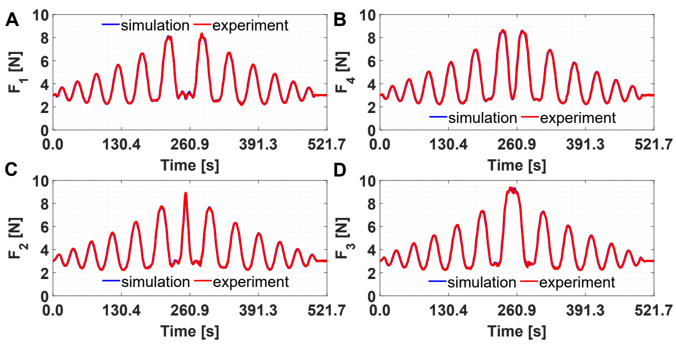

Fig. 12. Comparison of simulated and experimental cable tensions during tracking of the helical trajectory, with RMS errors below $0.09\,\mathrm{N}$.

on the system tracking capability. The LQR operating frequency range is estimated between 10 and $17\,\mathrm{Hz}$ depending on the tuning parameters. Accurate tracking is maintained for velocities up to 7–$8\,\mathrm{cm/s}$. Beyond this range, the controller bandwidth becomes insufficient to reproduce the required trajectory dynamics, leading to increased tracking errors and oscillations. The tested trajectories involve accelerations limited to $5.8\ \mathrm{cm/s^2}$ to ensure feasible cable tensions and stable tracking.

Additional delays arise from actuator dynamics and measurement filtering. The measured signals pass through first-order low-pass filters with time constants below $150\ \mathrm{ms}$, which introduce phase lag and slightly degrade high-frequency tracking performance during fast motions. Cable tension constraints also limit performance, as fast motions can induce large variations in cable forces, leading in some cases to tension saturation or loss of tension in one or more cables.

Overall, the proposed controller is based on a point-mass model and would need to be extended for a rigid platform. In this case, orientation dynamics must be included, and the system becomes underactuated. This would require an augmented state representation and more advanced control laws to handle coupled translational and rotational dynamics.

VI. Conclusion and Perspectives

This paper presents the experimental validation of an LQR controller with integral action for a suspended four-cable CDPR actuating a point mass. The proposed approach shows that linear optimal control can ensure stable and accurate 3D trajectory tracking in real time, despite gravity effects, cable tension constraints, and model nonlinearities. Compared to simulation-based studies such as [13], [14], this work provides an experimental demonstration of LQR-based control for suspended CDPRs without relying on nonlinear or predictive methods. Future work will focus on extending the proposed approach to rigid platforms, where orientation dynamics and underactuation must be considered, as well as incorporating more detailed cable and pulley models for large-scale CDPRs. In addition, trajectories with stopping points or sharp transitions may require careful design in cable-driven systems due to cable tension variations.

References

[1] M. Métillon, C. Charron, K. Subrin, and S. Caro, "Performance and interaction quality variations of a collaborative cable-driven parallel robot," *Mechatronics*, vol. 86, p. 102839, 2022.

[2] J.-M. Heo, B.-J. Park, J.-O. Park, C.-S. Kim, J. Jung, and K.-S. Park, "Workspace and stability analysis of a 6-dof cable-driven parallel robot using frequency-based variable constraints," *Journal of Mechanical Science and Technology*, vol. 32, no. 3, pp. 1345–1356, 2018.

[3] Y. Tadjouddine, J.-F. Antoine, A. A. Kumar, and T. Raharijaona, "Improving static workspace of a suspended cable-driven robot," in *26ème Congrès Français de Mécanique*, 2025.

[4] Y. Tadjouddine, J.-F. Antoine, A. Kumar, and T. Raharijaona, "Static workspace validation incorporating friction on a suspended reconfigurable cable-driven robot," *Mechatronics*, vol. 117, p. 103522, 2026.

[5] A. A. Kumar, J.-F. Antoine, and G. Abba, "Control of an underactuated 4 cable-driven parallel robot using modified input-output feedback linearization," *IFAC-PapersOnLine*, vol. 53, no. 2, pp. 8777–8782, 2020.

[6] E. Ida and M. Carricato, "Static workspace computation for underactuated cable-driven parallel robots," *Mechanism and Machine Theory*, vol. 193, p. 105551, 2024.

[7] M. Khosravi and H. D. Taghirad, "Stability analysis and robust pid control of cable driven robots considering elasticity in cables," *AUT Journal of Electrical Engineering*, vol. 48, no. 2, pp. 113–126, 2016.

[8] J. C. Santos, M. Gouttefarde, and A. Chemori, "A nonlinear model predictive control for the position tracking of cable-driven parallel robots," *IEEE Transactions on Robotics*, vol. 38, no. 4, pp. 2597–2616, 2022.

[9] A. Izadbakhsh, H. J. Asl, and T. Narikiyo, "Robust adaptive control of over-constrained actuated cable-driven parallel robots," in *International Conference on Cable-Driven Parallel Robots*. Springer, 2019, pp. 209–220.

[10] B. Zhang, W. Shang, B. Deng, S. Cong, and Z. Li, "High-precision adaptive control of cable-driven parallel robots with convergence guarantee," *IEEE Transactions on Industrial Electronics*, vol. 71, no. 7, pp. 7370–7380, 2023.

[11] R. Saadaoui, O. Piccin, G. I. Bara, and É. Laroche, "Modeling and control of a three degrees-of-freedom planar cable-driven parallel robot with flexible cables," *Journal of Dynamic Systems, Measurement, and Control*, vol. 147, no. 5, p. 051009, 2025.

[12] S. Abdolshah and E. Shojaei Barjuei, "Linear quadratic optimal controller for cable-driven parallel robots," *Frontiers of Mechanical Engineering*, vol. 10, no. 4, pp. 344–351, 2015.

[13] T. Garcia, D. Rémond, and S. Chesné, "Active damping of cable-driven parallel robots using lq command and measurement of cable tension variations," in *International Conference on Cable-Driven Parallel Robots*. Springer, 2025, pp. 92–103.

[14] Y. Hajjej, L. Boutat-Baddas, D. Martinez, M. P. Huertas-Ninos, A. Thabet, and M. Boutayeb, "On modelling and control of four cable suspended robots," in *2025 3rd International Conference on Control and Robot Technology (ICCRT)*. IEEE, 2025, pp. 30–36.

[15] A. Pott, *Cable-Driven Parallel Robots: Theory and Application*. Springer, 2018, vol. 120.

[16] J. Begey, L. Cuvillon, M. Lesellier, M. Gouttefarde, and J. Gangloff, "Dynamic control of parallel robots driven by flexible cables and actuated by position-controlled winches," *IEEE Transactions on Robotics*, vol. 35, no. 1, pp. 286–293, 2018.

[17] C. Jaen, J. Pou, R. Pindado, V. Sala, and J. Zaragoza, "A linear-quadratic regulator with integral action applied to pwm dc-dc converters," in *IECON 32nd Annual Conference on IEEE Industrial Electronics*. IEEE, 2006, pp. 2280–2285.